Compact Full-Duplex Amplify-and-Forward Relay Design for 5G Applications

Indrakshi Dey*, Zhixing Zhao†, M. Majid Butt‡ and Nicola Marchetti*
*CONNECT, Trinity College Dublin, Ireland
†Dept. of Electrical and Computer Engineering, University of Calgary
‡University of Glasgow, United Kingdom
Email: deyi@tcd.ie, zhaoz@ucalgary.ca, majid.butt@glasgow.ac.uk and nicola.marchetti@tcd.ie

***Abstract*—This paper presents a compact circuit design for implementing full-duplex relays serving network architectures envisioned for 5G applications. The proposed design prevents the transmit signal from interfering with the received signal through signal inversion. Signal inversion is accomplished through a compact design based on parametric amplifier circuit which operates simultaneously in two different modes, re-transmit and demodulate. This design also has an added advantage of being capable of generating phase difference between the transmitted and received signals by controlling the local oscillator signal. The validity of the design is evaluated against an example Smart Grid architecture, where it is employed to function as amplify-and-forward full-duplex relays/repeaters for serving several communication links. Simulation results indicate that full-duplex mode outperforms half-duplex one in terms of average channel capacity as well as bit error rate irrespective of the position of the relays with respect to distance from source/destination.**

I. Introduction

Emerging 5G applications like Internet-of-Things (IoT), Smart Grids, Smart Cities, etc., involve coexistence of multitude of end terminals like small wearable devices, automatic vehicles, industrial equipments. Connections between these end terminals and the base station or backhaul are served by small nodes like relays, repeaters, sensors and/or actuators. Network architectures that are served by relays/repeaters are termed as cooperative architectures, where the communication links can be bidirectional or unidirectional. The nodes desirably will be low-cost, easy-to-handle, energy-efficient and capable of multiple functionalities with minimum human intervention.

Full-duplex (FD) technology heavily features on the list of emerging technologies that meet the requirements of wireless data networks suitable for 5G applications [1]. Potential benefits of FD design include: a) increase in throughput, b) improvement in security and feedback, c) minimization of latency and d) elimination of hidden node and exposed node problems in contention-based networks. Despite its advantages, FD communication is plagued with residual self-interference, propagation path-loss, and cross-talk between transmitter and receiver [2].

Recent studies exhibited that it is critical to suppress or cancel self-interference and signal power attenuation imposed by the physical separation between two communicating devices and/or nodes to successfully address the shortcomings of FD communication [3]. Existing techniques concentrate on *isolation* (prevent RF-signal generated by the local transmitter from leaking onto its own receiver) [4], *cancellation* (subtract any remaining self-interference from the receive path using the knowledge of the transmit signal) [5] or a combination of the two [6]. Single-antenna based isolation techniques use circulators, which are considered to be bulky for below-6 GHz consumer equipments [7].

Self-interference cancellation includes digital cancellation [7], analog cancellation [8] and mixed-signal cancellation techniques [6]. Digital techniques cannot remove self-interference in the analog receiver chain and cannot prevent self-interference resulting from non-linear distortion or saturation. Analog techniques use noise cancellation chips to subtract self-interfering signal from the received signal. However, such techniques require precise knowledge of the self-interfering signal to achieve good levels of cancellation. Mixed-signal techniques require a dedicated additional up-converter that can introduce generic noise and distortion. The techniques that combine isolation with cancellation, require bulky components and/or antenna structures preventing their application to compact wireless FD nodes that can act as relays, sensors, etc.

Our work aims to solve the self-interference problem in FD nodes by focusing on a solution that can behave as an independent relay/repeater module. In order to accomplish that, we propose a compact single-antenna parametric amplifier based circuit design. This design enables the device to relay the information while demodulating the information for reception. The circuit is also capable of amplifying both the reflected and the demodulated signals with respect to the input signal. The novelty of our work lies in using these unique fea-

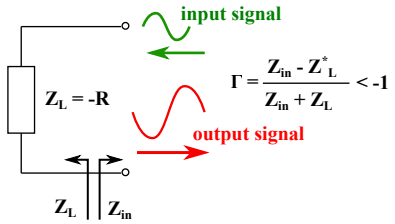

Fig. 1. Negative Impedance Amplifier Schematic Diagram.

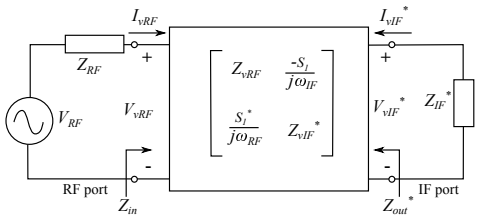

Fig. 2. Two-port Network Model of a Parametric Circuit. The LO signal is captured in the two-port Z-parameter representation of the parametric circuit. It is denoted by the parameter S_1. Therefore, the LO signal is not shown in the illustration.

tures for designing full-duplex relays/repeaters (FDRs). To the best of our knowledge, these benefits of parametric amplifier circuit have not been exploited to date for implementing FDRs in a real system architecture.

The proposed circuit has two major characteristics that minimize self-interference. Firstly, the received signal is inverted before re-transmission and secondly, the reflected and the demodulated signals are different in both frequency and phase. These features enable the circuit to operate in FD mode using a single antenna for transmission and reception. It minimizes the chance of any residual loop interference resulting from common approaches applying directional antennas [5] or balun cancellation [14], each of which uses separate antennas for transmission and reception. Besides, our proposed design is practically implementable in compact, low-cost IoT nodes (relays, sensors etc.), unlike physical isolation techniques [4] that require impractically large separation between transmit and receive antennas to reduce self-interference.

We implement and evaluate the performance of the proposed FD circuit design against one major 5G application, i.e. Smart Grid (SG), where the circuit is implemented as amplify-and-forward (AF) full-duplex relays/repeaters for serving the wireless communication links. We have selected SG architecture to test our design owing to its demands of achieving high system throughput while reducing energy consumption. Our proposed design improves system throughput using its full-duplexing capability. Besides, it inherently amplifies both the repeated and demodulated signals without requiring any additional amplifier .

For each source-to-destination link within the SG network, we set a choice of candidate relays and then opportunistically select the best candidate relay for transmission based on the instantaneous signal-to-interference-plus-noise ratio (SINR) of each cooperative link. Simulation results not only exhibit obvious performance improvement in FD case over half-duplex (HD) and non-cooperative scenarios, but also demonstrate that performance benefits can be achieved irrespective of the position of the relays (closer to source or closer to destination). This interesting feature can offer the flexibility of random positioning of relays to network operators in order to serve a wide coverage area.

The rest of the paper is organized as follows. Section II presents the detailed circuit design for the AF FD relay/repeater. Circuit-level performance of the proposed design and system-level performance analysis for an example SG architecture are provided in Section III and Section IV respectively. Concluding remarks are provided in Section V.

II. FD AF Relay Design

In this section, we describe the parametric amplifier circuit design that can be used to implement FDRs. In this case, the circuit has the ability to relay the information while deciphering the information for itself.

A. Basics of Parametric Amplifier

Parametric amplifier is a reactance amplifier that utilizes nonlinear reactance components, such as nonlinear capacitor or inductor, to achieve low-noise signal mixing and amplification [10]. To realize a signal amplification, negative impedance is generated. Thus, the parametric circuit can also be viewed as a negative impedance amplifier. The simplified conceptual diagram of a negative amplifier circuit is presented in Fig. 1. Circuit with negative impedance load always has a reflection coefficient smaller than -1, unlike circuits with positive impedance load, assuming both input impedance Z_{in} and load impedance Z_L are real. In other words, the input signal would gain energy and get reflected back depending on the denominator $(Z_{\text{in}} + Z_L)$ in the reflection coefficient Γ (refer to Fig. 1). As a result, the input signal to the circuit is inverted at the output and re-transmitted. Hence, the circuit can operate as an FD node with a single antenna reducing probability of residual loop interference plaguing prevalent FD solutions [4], [14] using separate transmit and receive antennas.

In our proposed design, we down-convert the input signal at frequency f_{RF} to an intermediate frequency (IF) signal at $f_{IF} = f_{LO} - f_{RF}$, where f_{LO} is the local oscillator (LO) frequency. By tuning the combination of the source and load impedances (Z_S and Z_L respectively) as well as f_{RF} and f_{IF}, the circuit can offer negative impedance at both the RF

$$\Gamma_{RF} = \frac{\left\{R_s - \frac{|S_1|^2}{\omega_{RF}\omega_{IF}} \frac{R_s+R_{IF}}{(R_s+R_{IF})^2+[X_{IF}-\frac{S_0}{\omega_{IF}}]^2} - R_{RF}\right\} - j\left\{\frac{S_0}{\omega_{RF}} + \frac{|S_1|^2}{\omega_{RF}\omega_{IF}} \frac{X_{IF}-(S_0/\omega_{IF})}{(R_s+R_{IF})^2+[X_{IF}-\frac{S_0}{\omega_{IF}}]^2} - X_{RF}\right\}}{\left\{R_s - \frac{|S_1|^2}{\omega_{RF}\omega_{IF}} \frac{R_s+R_{IF}}{(R_s+R_{IF})^2+[X_{IF}-\frac{S_0}{\omega_{IF}}]^2} + R_{RF}\right\} - j\left\{\frac{S_0}{\omega_{RF}} + \frac{|S_1|^2}{\omega_{RF}\omega_{IF}} \frac{X_{IF}-(S_0/\omega_{IF})}{(R_s+R_{IF})^2+[X_{IF}-\frac{S_0}{\omega_{IF}}]^2} - X_{RF}\right\}} \quad (1)$$

and IF output ports simultaneously, i.e. $\Re\{Z_L\}$ and $\Re\{Z_{\text{out}}\}$ are both negative, where '$\Re$' represents the real part of a complex variable. Using the negative impedances, $\Re\{Z_L\}$ and $\Re\{Z_{\text{out}}\}$, both the reflected and the demodulated signals are amplified with respect to the input signal. Therefore, this circuit can be implemented as a compact single-antenna FD relay-cum-receiver, especially for IoT-like applications, a novelty that has never been explored in literature.

For a parametric amplifier circuit with a negative impedance termination, the input signal wave is amplified and reflected. Therefore, the reflected signal at f_{RF} is boosted. It is worth-mentioning here that the parametric amplifier operation matches the common frequency-mixer configuration. It uses the LO signal at f_{LO} to realize signal mixing and this LO signal is responsible for the RF signal amplification. That is the power in LO signal contributes to the power gain in the RF signal. In fact, thanks to the enhancement in RF signal, the IF signal is also improved or a frequency conversion power gain is obtained. This unique feature will be used to design and implement FDRs in the next subsection.

B. Parametric Circuit in AF mode

The two-port network model of a parametric circuit operating in FD mode can be represented as in Fig. 2. The input signal to the parametric circuit gets re-transmitted at the same frequency, while simultaneously being demodulated back to baseband. Therefore, our proposed FDR circuit operates in two different modes: a) Repeat/Re-transmission and b) Demodulation, both of which are executed simultaneously. A detailed analysis of both modes of operation is provided below separately.

1) Repeating/Re-transmitting: This mode of the FDR circuits behaves as a negative impedance amplifier, as shown in Fig. 1. The input power P_{in} and the reflected power P_{out} comply with the relationship $P_{\text{out}} = |\Gamma|^2 P_{\text{in}}$ [12]. Since we are dealing with a negative impedance amplifier, the real part of Z_L is negative. Thus $|\Gamma|^2 > 1$ and hence, $P_{\text{out}} > P_{\text{in}}$.

The power gain realization at f_{RF} is due to the introduction of a negative impedance. Applying harmonic balance analysis and only taking first-order equation into consideration, we obtain a conversion matrix representing the nonlinear capacitor and it is formulated as [11],

$$\begin{bmatrix} V_{vRF} \\ V^*_{vIF} \end{bmatrix} = \begin{bmatrix} R_s + \frac{S_0}{j\omega_{RF}} & \frac{-S_1}{j\omega_{IF}} \\ \frac{S^*_1}{j\omega_{RF}} & R_s - \frac{S_0}{j\omega_{IF}} \end{bmatrix} \begin{bmatrix} I_{vRF} \\ I^*_{vIF} \end{bmatrix} \quad (2)$$

where V_{vRF}, V_{vIF}, I_{vRF}, and I_{vIF} are the voltages and currents at ω_{RF} and ω_{IF} respectively and '$*$' represents the complex-conjugate. In (2), R_s is the internal resistance of the varactor, S_0 and S_1 are the average elastance and the first harmonic of Fourier series expansion of the varactor elastance respectively[1]. Using two-port network theory and applying Kirchhoff's Voltage Law (KVL) and Kirchhoff's Current Law (KCL) to Fig. 2, the input and output impedance can be calculated as,

$$Z_{\text{in}} = Z_{vRF} - \left(|S_1|^2/(\omega_{RF}\omega_{IF}(Z^*_{vIF} + Z^*_{IF})\right) \quad (3)$$

$$Z_{\text{out}} = Z^*_{vIF} - \left(|S_1|^2/(\omega_{RF}\omega_{IF}(Z_{vRF}+Z_{RF}))\right) \quad (4)$$

where $Z_{vRF} = R_s + S_0/(j\omega_{RF})$ and $Z_{vIF} = R_s + S_0/(j\omega_{IF})$.

Since RF signal is considered only in the repeating mode, we can treat the parametric circuit as an equivalent impedance, Z_{in} (refer to Fig. 2) according to Thevenin theorem. Thus, the reflection coefficient at RF port can be expressed as [12],

$$\Gamma_{RF} = \frac{Z_{\text{in}} - Z^*_{RF}}{Z_{\text{in}} + Z_{RF}} \quad (5)$$

Therefore, **power gain** in repeating mode can be obtained as,

$$G_r = P_{\text{out}}/P_{\text{in}} = |\Gamma_{RF}|^2. \quad (6)$$

2) Demodulating: If the output signal is selected from the IF port of Fig. 2, then the FDR circuit operates as a demodulator. In this demodulating mode, the parametric circuit acts as a frequency mixer where the input RF signal is down-converted to IF signal using the LO signal.

In literature [12], there are several definitions of the power gain for a demodulator circuit. Among them the **transducer gain** (the ratio of the delivered output power to the available input power) is considered as a generic indicator for the power utilization efficiency

[1]The elastance is the reciprocal of capacitance. It is introduced for the simplicity of calculations.

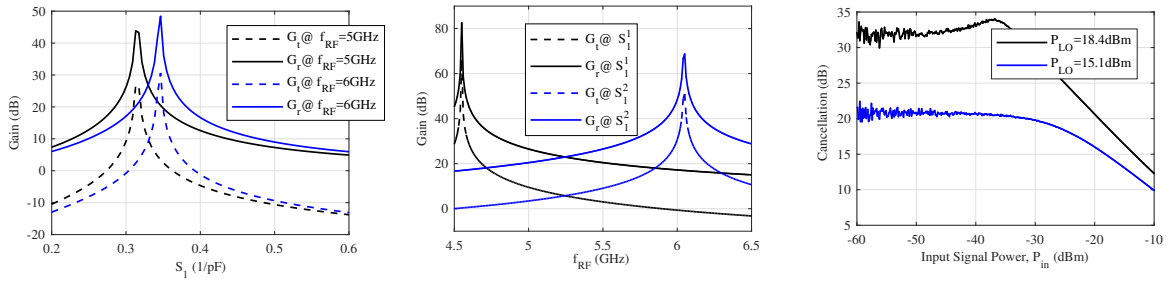

(a) Power gains of repeater G_r and demodulator G_t for S_1 values at different f_{RF}.

(b) Power gains G_r and G_t against f_{RF} at $S_1^1 = 0.31$ (1/pF) and $S_1^2 = 0.346$ (1/pF).

(c) Cancellation performance against received power for a 10 MHz wide input signal at $f_{RF} = 6$ GHz.

Fig. 3. Circuit level performance of proposed FDR parametric circuit design.

of the circuit. In this paper, we consider the transducer gain which is formulated as,

$$G_t = \frac{P_L}{P_{in}} = \frac{4\Re(Z_{RF})\Re(Z_{IF})(|S_1|^2/\omega_{RF}^2)}{\left|(Z_{RF}+Z_{vRF})(Z_{IF}^*+Z_{vIF}^*) - \frac{S_1^2}{\omega_{RF}\omega_{IF}}\right|^2} \quad (7)$$

where P_L is the delivered load power.

From the analysis above, it can be intuitively concluded that S_1 has a profound impact on the performance of the parametric circuit and it is associated with LO signal power level. As a rule of thumb, the stronger LO signal is, the larger the value of S_1 is. Therefore, the LO signal is an essential knob of the parametric circuit. It controls both the repeater and demodulator gains. In fact, it can also adjust the phase difference between the input and reflected signals at f_{RF}.

3) Phase Difference between transmit and receive signals: The input power wave a_1 and reflected power wave b_1 at the RF port of the parametric circuit comply with the following relationship [12],

$$b_1 = a_1\Gamma_{RF}. \quad (8)$$

where a_1 and b_1 are complex numbers that contain both magnitude and phase information. Therefore, the phase difference between the input and reflected power waves is entirely dependent on the reflection coefficient, Γ_{RF}.

Assuming $Z_{RF} = R_{RF} + jX_{RF}$ and $Z_{IF} = R_{IF} + jX_{IF}$, putting these values in (5) and then isolating the real and imaginary part, we can obtain the expression for Γ_{RF} in (1). It is clear from (1) that the phase difference between the incident and the reflected waves can be manipulated through control of S_1 (that is by adjusting LO signal). Depending on the application scenario (i.e. for different values of Z_{in}, Z_{out} and Z_L), this design can potentially attain required amplification of the input signal and preferable phase difference between input and output signals.

III. Circuit-Level Simulation

Fig. 3 presents circuit-level simulation results where the curves are generated by varying f_{RF} from 4.5 GHz to 6 GHz (refer to Fig. 3(a) and Fig. 3(b)). Only for Fig 3(c), f_{RF} is kept constant at 6 GHz. For simulation, f_{IF} is chosen to be fixed at 0.1 GHz. In order to obtain signal amplification in both retransmitting and demodulating modes, f_{LO} is chosen such that f_{LO} = f_{RF} + f_{IF} is satisfied. We also assume that average capacitance of the varactor of the parametric circuit is canceled out at both f_{RF} and f_{IF}.

The varactor is chosen from the library of 0.13-μm bulk CMOS technology. Only the capacitor vs. voltage characteristic is extracted from the chosen varactor, based on which the parameters used in the simulation are extrapolated. It is worth mentioning here that as we have used a realistic varactor model which contains a lossy part (i.e. $\Re\{R_s\}$ is taken into account in all equations derived earlier). Though $\Re\{R_s\}$ is quite small, it plays a critical role in evaluation of simulated gain performance.

Fig. 3(a) shows that gains for both demodulator and repeater have same optimal point. For this S_1 sweep simulation, we have varied S_1 from 20 to 80 % of its maximum possible value. One interesting feature we can obtain from this is that with control of S_1 or LO signal magnitude, the circuit becomes frequency-selective. In other words, one can level the LO power to make the circuit work at different carrier frequencies.

Similarly Fig. 3(b) exhibits the gain performance of both the repeater and demodulator modes against frequency for given values of S_1. It again demonstrates that both repeater and demodulator have the same optimal points. However, for each set of S_1 values, the repeater gain tends to be higher than that of the demodulator. This particular feature is advantageous for real circuit implementation because we obtain inherently higher gain at high frequency output (i.e., repeater output). For the low frequency output (i.e.,

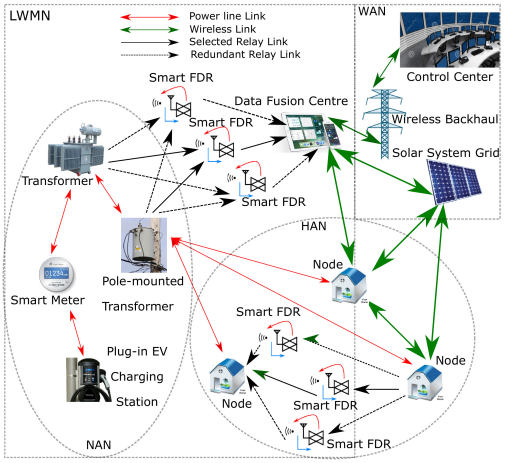

Fig. 4. Smart Grid Architecture (*Abbr. ref. : FDR - Full-Duplex relays, EV - electric vehicles, HAN - home area network, NAN - neighborhood area network, LWMN - local wireless mesh network, WAN - wide area network*)

demodulator output), we can easily boost the signal by integrating a baseband amplifier with a low cost.

The Fig. 3(c) shows how much the self-interfering signal (re-transmitted signal from the RF port leaking into the received signal at the input port) is attenuated due to signal inversion by the parametric circuit. The f_{RF} is chosen to be 6 GHz with a bandwidth of 10 MHz. We chose 6 GHz input signal for generating these results since a high G_r of 49 dB is obtained at 6 GHz (refer to Fig. 3(a)). About 35 dB of cancellation is achieved at lower receive powers which reduces to around 10 dB with increase in receive power to about -10 dBm. The amount of cancellation also depends on the LO power, P_{LO} with cancellation performance improving with increase in P_{LO}. Therefore, our circuit offers a higher self-interference cancellation than the recently proposed balun active cancellation [14] by around $5 \sim 10$ dB and at the same time, has the flexibility to control the amount of cancellation by adapting P_{LO}.

It is worth-mentioning that these are simulation results, and present only a glimpse of how the real circuit will perform. Detailed implementation and measurement of the actual circuitry is beyond the scope of this paper.

IV. System-Level Performance Analysis

We include the AF FDR behavioral model proposed in Section II in a baseband simulation of an SG application scenario served by a number of one-way FDRs, represented in Fig. 4. Here we consider an SG architecture [9], where, home area networks (HANs), neighborhood area networks (NANs) and local electric equipments are connected to form a local wireless mesh network (LWMN). The data fusion center acts as an access point for each LWMN. Each data fusion center is connected to an existing wide area network (WAN) which acts as backhaul. In addition to the existing nodes, a limited number of FDRs are also deployed in the network to exploit diversity gain and cooperative transmission opportunistically. For each cooperative link in the SG network, a candidate set of $\mathcal{M}$ number of relays are available. From this set, the single best relay having the highest end-to-end (source (S) - relay and relay - destination (D)) channel quality is selected and hence, we refer to such relays as smart FDRs.

For generating the simulation results, we consider a 16 Quadrature Amplitude Modulation (16-QAM) signal generated by S at a center frequency of 6 GHz and signal bandwidth of 10 MHz. We choose 16-QAM as our preferred modulation technique as it can achieve moderately low BER in a flat fading propagation environment.

The instantaneous fading channel coefficients over both cooperative h_{sr_i} (S $\rightarrow$ ith FDR), $h_{r_i d}$ (ith FDR $\rightarrow$ D) for $1 \leq i \leq \mathcal{M}$ and non-cooperative h_{sd} (S $\rightarrow$ D) links are assumed to be non-selective double-Rayleigh distributed such that each of the fading coefficients is a product of two independent complex Gaussian random variables, ξ and λ, with zero mean and variance of 0.5 per dimension. We choose double-Rayleigh distribution to model the wireless links as it is shown to characterize outdoor cooperative links appropriately in urban and sub-urban scenarios in [13].

We take into account three types of cooperative links. The distance between each source and ith smart FDR is given by d_{sr_i} (e.g., the link between the transformer and one FDR in Fig. 4). The distance between ith FDR and destination is given by $d_{r_i d}$ (e.g., the link between one FDR and the data fusion center in Fig. 4). The direct link distance between each set of source and destination is given by d_{sd} (i.e. the direct distance between the transformer and the data fusion center in Fig. 4). We take into account 3 sets of such source and destination links in our considered SG architecture for generating the simulations results.

The received signal at the ith FDR is expressed as,

$$y_{r_i} = h_{sr_i}\sqrt{P_s}x_s + h_i\sqrt{P_{r_i}}x_{r_i} + n_{r_i} \qquad (9)$$

where $h_i \sim \mathcal{CN}(0, \sigma_i^2)$ is the residual self-interference at the ith FDR, x_s and x_{r_i} are the transmitted signals from S and ith FDR respectively, $P_s = \zeta_s\left(\frac{d_{\min}}{d_{sr_i}}\right)^{\eta_s}$ and $P_{r_i} = \zeta_{r_i}\left(\frac{d_{\min}}{d_{r_i d}}\right)^{\eta_{r_i}}$ are the transmit powers from S and ith FDR respectively such that η_s, η_{r_i} are the respective pathloss exponents, $10\log_{10}(\zeta_s) \sim \mathcal{N}(\mu_s, \sigma_s^2), 10\log_{10}(\zeta_{r_i}) \sim \mathcal{N}(\mu_{r_i}, \sigma_{r_i}^2)$ are the respective log-normal distributed shadowing values, $d_{\min}$ is the minimum distance encountered between any of

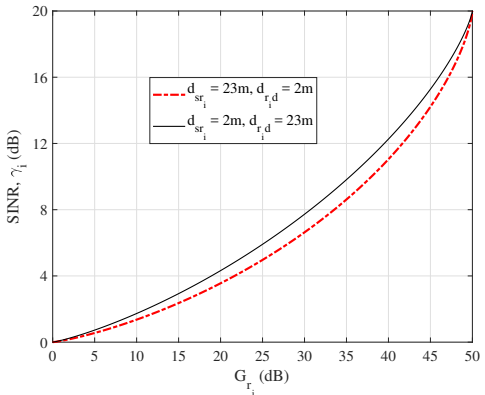

Fig. 5. Signal-to-interference plus noise ratio in the ith full-duplex relay link in terms of the relay gain for a 25m S $\rightarrow$ R_i $\rightarrow$ D link for 10 MHz wide 16-QAM modulated signal at an operating frequency of 6 GHz.

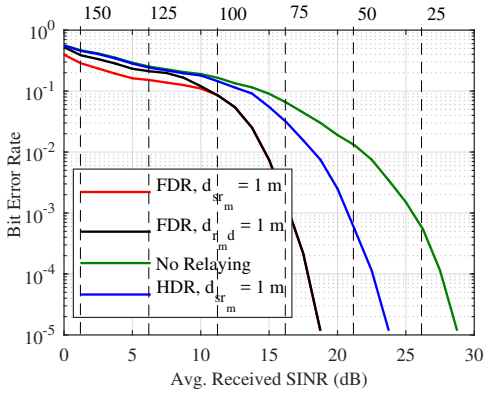

Fig. 6. System BER performance for the considered SG architecture as a function of SINR, where the dashed vertical lines represent distances between S and D, $d_{sd} = \{150, 125, 100, 75, 50, 25\}$ m.

the available FDRs and either S or D, and $n_{r_i} \sim \mathcal{N}(0, N_0)$. The received signal at D is obtained as,

$$y_d = h_{r_id}\sqrt{P_{r_i}}x_{r_i} + h_{sd}\sqrt{P_s}x_s + n_d \tag{10}$$

with $x_{r_i} = G_{r_i}y_{r_i}$ and $n_d \sim \mathcal{N}(0, N_0)$, where G_{r_i} is the repeater gain (amplification factor) obtained from the parametric circuit of the ith FDR. Therefore, the end-to-end SINR over the ith FDR link is given by,

$$\gamma_i = \frac{P_s P_{r_i}|h_{sr_i}|^2|h_{r_id}|^2}{\frac{N_0}{G_{r_i}^2} + \left(N_0 + \frac{P_{r_i}|h_i|^2(P_s|h_{sr_i}|^2+N_0)}{1/G_{r_i}^2 - P_{r_i}|h_i|^2}\right)P_{r_i}|h_{r_id}|^2} \tag{11}$$

with $|h_{sd}|^2 \approx 0$ due to high attenuation experienced by the signal over the direct link between S and D [15]. It is to be mentioned here that the direct link connectivity does not affect the relay selection and all the FDRs are one-way FD nodes. It is also worth mentioning that this direct link adds diversity to the system and can be exploited for performance benefits, the analysis of which is beyond the scope of this paper. Assuming all noise components are Gaussian distributed with equal variance of N_0, the average end-to-end capacity over the ith FDR link can be calculated as,

$$C_{r_i}^{\text{FD}} = \mathcal{E}_{h_{r_id}}\{\log_2(1+\gamma_i)\} \tag{12}$$

where $\mathcal{E}$ denotes expectation. Using optimal relay selection policy, the selected mth relay for transmission will satisfy,

$$m = \underset{i}{\text{argmax}}\{\gamma_i\} \tag{13}$$

for $1 \leq i \leq \mathcal{M}$ [15]. Using this selection relaying scheme, we simulate BER performance and achievable capacity limit for the SG architecture presented in Fig. 4. For simulation purposes, we use $\eta_s = \eta_{r_i} = 2.5$, $\mu_s = \mu_{r_i} = 10$ and $\sigma_s = \sigma_{r_i} = 2$ (representing dense urban scenarios) [16]. For residual self-interference at each FDR, we consider $\sigma_i^2 = \{\sigma_1^2, \ldots, \sigma_{\mathcal{M}}^2\} = 0.08$, where σ_i^2 is the variance of the loop interfering channel h_i (refer to (9)). We also assume that FDRs are uniformly deployed on a 2-D (2-dimensional) circular plane around S or D with maximum and minimum radii of $d_{\max} = 10$ m and $d_{\min} = 1$ m respectively. For comparison purposes, we compare the FDR performance to that of a system with half-duplex AF opportunistic relaying.

Fig. 5 illustrates the end-to-end SINR γ_i (dB) of the ith FDR link positioned at a distance of 2 m from either S or D as a function of the corresponding repeater gain G_{r_i} (dB). Two sets of results are generated, one for $d_{sr_i} = 2$ m and $d_{r_id} = 23$ m, other for $d_{sr_i} = 23$ m and $d_{r_id} = 2$ m. The results show that it is more advantageous to place the relays close to S than placing them close to D. However, the amount of performance benefit achieved is a negligible SINR increase of 0.5 to 1 dB. For a G_{r_i} higher than 50 dB, performance benefits can be achieved irrespective of the relay location.

The BER performance (Fig. 6) and achievable capacity (Fig. 7) results for the considered SG architecture are simulated as a function of the average received SINR. The average received SINR in these cases refer the SINR received over all the opportunistically selected relay to destination links (3 in total) and is calculated using $\frac{\text{E}\{|h_{r_md}|^2\}}{\text{E}\{|h_m|^2\}+N_0}$ for each link, where N_0 is the variance of the total additive white Gaussian noise (AWGN) afflicting the destination.

From Fig. 6, it is evident that for every increase in d_{sd} by 25 m, the BER degrades by one or two orders of magnitude, even at high SINR values. At low SINR values, placing the relay closer to the source (the case where $\min d_{sr_i} = 1$ m) is advantageous over placing the relay closer to the destination (the case where $\min d_{r_id} = 1$ m). However, at higher SINR, both the conditions result in an equivalent BER performance. Both the FD modes of operation also perform better than the HD mode in terms of BER. The

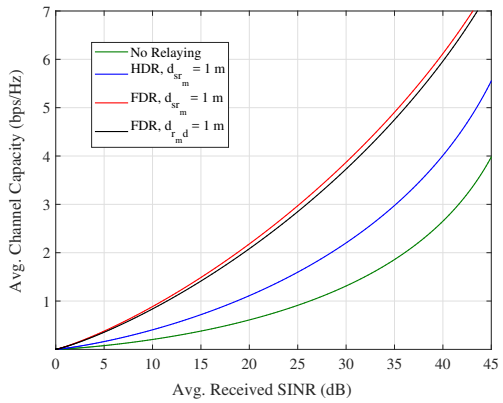

Fig. 7. Average channel capacity for the considered SG architecture using opportunistic FD AF relaying as a function of average received SINR, where all the FDRs offer equal amplification G_{r_i} = 50 dB.

reason can be attributed to the fact that the parametric circuit acting as FDR inverts the input signal from S before re-transmitting it to D yielding negligible self-interference. For all candidate FDRs, the amplification factor of AF relaying is kept fixed with an available power gain at the repeater port as $G_{r_i} = 50$ dB. The number of candidate relays for opportunistic relaying in the FDR cases of Fig. 6 are chosen to be 6 for all scenarios.

The set of results in Fig. 7 are generated by plotting the average channel capacity as a function of average received SINR with $\mathcal{M} = 6$ between each set of source and destination link with a total of 3 such links. In Fig. 7, it is assumed that the relays are uniformly deployed over a 2-D circle with radius between $d_{\max}$ and $d_{\min}$ and S or D of the link is at the center of the circle. The FD modes outperform HD mode for opportunistic cooperative communication in all cases. With the increase in SINR, more loop interference is tolerated by the FD modes yielding around 80% increase in capacity for average received SINR between 30 and 40 dB over the HD alternative irrespective of the closeness of the relay to S or D.

V. Conclusion

The main contribution of this paper is to design portable FD relays/repeaters using parametric amplifier. The major advantage of this circuit is its capability of inverting the receive signal before re-transmission, thereby minimizing self-interference. This feature also enables the circuit to transmit and receive through a single antenna lowering residual loop interference common in existing physical isolation-based solutions. The performance of the circuit is examined in terms of the BER metric and average channel capacity, where this design is employed to act as an AF FDR as a part of Smart Grid network architectures envisioned under 5G. Simulated performance reveals its benefits over HD and non-cooperative scenarios. Improvement in BER and channel capacity can be achieved through opportunistic relaying irrespective of the proximity of the relays to source or destination, where each source-to-destination link is served by more than one candidate relay. This eliminates the requirement of optimizing the relay location to enhance system performance.

Acknowledgment

This work is supported by the EDGE grant 13236/203377 under Marie Skodowska-Curie CO-FUND Actions.

References

[1] J. I. Choi, M. Jain, K. Srinivasan, P. Levis, and S. Katti, "Achieving single channel, full duplex wireless communication," in *Proc. Int. Conf. Mobile Comput. Netw.*, 2010, pp. 1–12.

[2] M. S. Amjad et al., "A Low-Complexity Full-Duplex Radio Implementation With a Single Antenna," *IEEE Transactions on Vehicular Technology*, vol. 67, no. 3, pp. 2206–2218, Mar. 2018.

[3] P. C. Weeraddana et al., "On the effect of self-interference cancellation in multihop wireless networks," *J. Wireless Commun. Netw.*, vol. 2010, pp. 1–10, 2010.

[4] S. Chen et al., "Division-free duplex for wireless applications," *IEEE Electron. Lett.*, vol. 34, no. 2, pp. 147–148, Jan. 1998.

[5] M. Duarte et al., "Design and characterization of a full-duplex multi-antenna system for WiFi networks," *IEEE Trans. Veh. Technol.*, vol. 63, no. 3, pp. 1160–1177, Mar. 2014.

[6] A. Sahai, G. Patel, C. Dick, and A. Sabharwal, "Understanding the impact of phase noise on active cancellation in wireless full-duplex," in *Proc. Asilomar Conf. Signals, Syst. Comput.*, 2012, pp. 29–33.

[7] D. Bharadia, E. McMilin, and S. Katti, "Full duplex radios," in *Proc. ACM Special Interest Group Data Commun.*, 2013, pp. 1–12.

[8] A. Sahai et al., "On the impact of phase noise on active cancellation in wireless full-duplex," *IEEE Trans. Veh.Technol.*, vol. 62, no. 9, pp. 4494–4510, Nov. 2013.

[9] M. H. U. Ahmed et al., "Smart grid cooperative communication with smart relay", in *IEEE Journal of Communications and Networks*, vol. 14, no. 6, Dec. 2012, pp. 640–652.

[10] Z. Zhao et al., "Parametric CMOS upconverters and downconverters," in *Int. J. Circ. Theor. Appl.*, vol. 42, no. 12, Dec. 2014, pp. 1209–1227.

[11] S. A. Maas, *Nonlinear Microwave Circuits*, 1st Edition. USA : John Wiley & Sons, 1996.

[12] D. M. Pozar, *Microwave Engineering*, 2nd Edition. USA: John Wiley & Sons, 1998.

[13] I. Dey et al., "Performance analysis of relay-assisted mobile-to-mobile communication in double or cascaded rayleigh fading," in *Proc. IEEE PACRIM*, Victoria, Canada, pp. 631–636, Aug. 2011.

[14] M. Jain et al., "Practical, real-time, full duplex wireless," in *MobiCom 2011*, pp. 301–312, New York, NY, USA, 2011. ACM.

[15] Q. Li, S. Feng, X. Ge, G. Mao, and L. Hanzo, "On the Performance of Full-Duplex Multi-Relay Channels With DF Relays," *IEEE Transactions on Vehicular Technology*, vol. 66, no. 10, pp. 9550–9554, Oct. 2017.

[16] M. W. Wasson et al., "Dense urban channel measurements for utility pole fixed wireless links," *IEEE Trans. Antennas Propag.*, vol. 63, no. 12, pp. 5791–5798, Dec. 2015.